

Internal Robustness: systematic search for systematic bias in SN Ia data

Luca Amendola¹, Valerio Marra¹ and Miguel Quartin²

¹*Institut für Theoretische Physik, Universität Heidelberg, Philosophenweg 16, 69120 Heidelberg, Germany*

²*Instituto de Física, Universidade Federal do Rio de Janeiro, CEP 21941-972, Rio de Janeiro, RJ, Brazil*

Accepted XXX. Received XXX; in original form XXX

ABSTRACT

A great deal of effort is currently being devoted to understanding, estimating and removing systematic errors in cosmological data. In the particular case of type Ia supernovae, systematics are starting to dominate the error budget. Here we propose a Bayesian tool for carrying out a systematic search for systematic contamination. This serves as an extension to the standard goodness-of-fit tests and allows not only to cross-check raw or processed data for the presence of systematics but also to pin-point the data that are most likely contaminated. We successfully test our tool with mock catalogues and conclude that the Union2.1 data do not possess a significant amount of systematics. Finally, we show that if one includes in Union2.1 the supernovae that originally failed the quality cuts, our tool signals the presence of systematics at over $3.8\text{-}\sigma$ confidence level.

Key words: methods: statistical – cosmology: cosmological parameters – stars: supernovae: general

1 INTRODUCTION

The best evidence for the accelerated expansion of the universe still comes, after 15 years from the earliest results (Riess et al. 1998; Perlmutter et al. 1999), from the supernovae Ia (SNIa). There are now several hundreds SNIa useful for cosmological purposes, ranging in distance up to $z \approx 1.7$. The SNIa have been compiled in different datasets (Kowalski et al. 2008; Hicken et al. 2009; Lampeitl et al. 2009; Guy et al. 2010; Conley et al. 2011; Suzuki et al. 2012), taking into account different sets of possible systematics and making use of two different approaches to standardize these primordial candles (Jha et al. 2007; Guy et al. 2007). Nevertheless, every analysis performed on these datasets confirms that a present cosmic acceleration explains satisfactorily the data. The same conclusion is now supported also by several other lines of evidence, such as measurements of the Baryonic Acoustic Oscillations (BAO) (Eisenstein et al. 2005; Blake et al. 2011), of the anisotropies of the Cosmic Background Radiation (CMB) (Komatsu et al. 2011) and of the age of the oldest stars known (Jimenez et al. 1996; Carretta et al. 2000; Hansen et al. 2002).

The recent increase in the number of observed supernovae is also driving a huge effort to understand and control possible sources of systematics that may undermine the progress in the cosmological interpretation. A recent analysis (Suzuki et al. 2012) claims indeed the systematic uncertainties are already larger than the statistical ones and

the issue will be much more important in the near future as we forecast an increase in the number of observed supernovae by 1 order of magnitude in the next ~ 5 years (for example with the Dark Energy Survey, see Bernstein et al. 2009) and by 2 orders of magnitude in the next ~ 15 (for example with the Large Synoptic Survey Telescope, see Abell et al. 2009). It is thus necessary to continue investigating the SNIa datasets in search of such systematic effects and of additional cosmological information. On one side, in fact, we are already aware of many effects that could come into play to alter the SNIa apparent magnitude: contamination from non-Ia supernovae, dust absorption in both host galaxy and Milky Way, gravitational lensing distortions, local velocity flows *et cetera*; not to count systematics which arise from selection effects (Kainulainen & Marra 2009, 2011a,b) and from relying solely on photometry (typically in just a few bandpasses) and the flux reference of such filters (for a review, see for instance Howell 2011). On the other side, non standard cosmological models might affect our parameter estimation: for instance, any anisotropy in the expansion rate would show up as an anisotropy in the SNIa cosmological parameters. There have been of course many searches for such systematic biases. All of them, however, assume a specific effect (say, gravitational lensing as in Amendola et al. 2010 or cosmological anisotropy as in Koivisto et al. 2011; Antoniou & Perivolaropoulos 2010; Colin et al. 2011) and test whether this effect is enough to make some SNIa

incompatible with the others. In other words, one proceeds by testing a specific prejudice.

In this paper we propose an alternative approach. We wish to perform a systematic search of biases without having any preferred selection criteria. In other words, we try to answer the following question: is there any subset of SNIa that is statistically incompatible with the others? That is, is there a subset of SNIa that could be described by parameters which are incompatible with those that describe the other SNIa? In a sense, this is a direct generalization of the search for outliers. Instead of searching for single outliers, i.e. SNIa that appear statistically incompatible with the others (say, some parameters that describe their light curves are too far off from the others or their distance moduli just end up very far from the overall Hubble diagram), we search for subsets of, say, dozens of SNIa at once whose parameters are incompatible with the others. In other words, we search for heteroscedasticity in the SNIa data. As will be shown in Section 2.2, the proposed generalization reduces to the standard outlier search in the limit in which the whole data is divided into two complementary datasets, one of which contains a single element.

The standard tool to compare whether a particular dataset is compatible with a proposed model is the *goodness-of-fit* test, which gives well defined probability statements about such agreement. However, the information obtained is limited, and this simple analysis may hide problems in both data and model. For instance, if a given model parameter affects only a small fraction of the data, even if such parameter turns out to disagree with this fraction the goodness-of-fit may still claim an overall good fit. To address this issue, a modification of the test, dubbed *parameter goodness-of-fit*, was proposed in Maltoni et al. 2002 and later extended in Maltoni & Schwetz 2003. The parameter goodness-of-fit method nevertheless still relies on comparisons of χ^2 values which are only sensitive to the local minimum, and not to the entire likelihood. Here, instead, we will adopt a fully Bayesian approach so as to use all the information available, e.g. a possible overlapping of the likelihoods surfaces. We dub *internal robustness* the fundamental quantity evaluated in this method. The name is motivated by the analogous quantity *robustness* which was recently defined by March et al. 2011 (and originally introduced in Marshall et al. 2006) in a context in which the two datasets refer to different observational probes (and which we will henceforth refer to as *external robustness*, for differentiation). In particular, March et al. 2011 showed that the robustness is an estimator “orthogonal” to the Figure of Merit, which is sensitive to the relative orientation of the two probes but not to the distance between the two-experiment confidence regions.

This paper is organized as follows. In Section 2 we will introduce the formalism of the internal robustness. In Section 3 we will describe how we will systematically search for bias in SNe data. In Section 4 we will show the results relative to a biased test catalogue, the Union2.1 catalogue augmented with the supernovae that did not pass the quality cuts, and the actual Union2.1 dataset. As we will see, our method will be able to detect the systematic bias in the first two catalogues. Moreover, our analysis does not show signs of systematic effects in the actual Union2.1 catalogue. Finally, we will give our conclusions in Section 5, and explain some technical details in Appendix A.

We will adopt the following notation. Bold face will distinguish a vector \mathbf{x} or matrix \mathbf{A} from their components x_i and A_{ij} , a superscript t will denote a transposed vector or matrix, $|\mathbf{A}|$ will represent the determinant of a matrix \mathbf{A} , and a hat will indicate the best-fit value of the corresponding quantity.

2 FORMALISM

2.1 Bayesian evidence and its Fisher approximation

Let us first of all recall some statistical definitions in the Bayesian context (Trotta 2008; Amendola & Tsujikawa 2010). The Bayesian *evidence* is defined as

$$\mathcal{E}(\mathbf{x}; M) = \int \mathcal{L}(\mathbf{x}; \boldsymbol{\theta}^M) \mathcal{P}(\boldsymbol{\theta}^M) d^n \boldsymbol{\theta}^M, \quad (1)$$

where $\mathbf{x} = (x_1, x_2, \dots, x_N)$ are N random data, $\boldsymbol{\theta}^M = (\theta_1, \theta_2, \dots, \theta_n)$ are n theoretical parameters that describe the model M , \mathcal{L} is the likelihood function, and \mathcal{P} is the prior probability of the parameters $\boldsymbol{\theta}^M$. If $\mathcal{P}(M)$ is the prior on a particular model M , we can use Bayes’ theorem to write

$$\mathfrak{L}(M; \mathbf{x}) = \mathcal{E}(\mathbf{x}; M) \frac{\mathcal{P}(M)}{\mathcal{P}(\mathbf{x})}, \quad (2)$$

i.e. the posterior probability \mathfrak{L} of having model M given the data. We can finally use the latter equation to compare quantitatively two models taking the ratio of their probabilities (so that $\mathcal{P}(\mathbf{x})$ cancels out):

$$\frac{\mathfrak{L}(M_1; \mathbf{x})}{\mathfrak{L}(M_2; \mathbf{x})} = \mathcal{B}_{12} \frac{\mathcal{P}(M_1)}{\mathcal{P}(M_2)}, \quad (3)$$

where we introduced the Bayes ratio (sometimes referred to as Bayes factor)

$$\mathcal{B}_{12} = \frac{\mathcal{E}(\mathbf{x}; M_1)}{\mathcal{E}(\mathbf{x}; M_2)}. \quad (4)$$

Often, however, one assumes that $\mathcal{P}(M_1) = \mathcal{P}(M_2)$ and we adopt this choice here. A Bayes ratio $\mathcal{B}_{12} > 1$ (< 1) says that current data favors the model M_1 (M_2). As we will see in the next Section the Bayes ratio will be central in the definition of *internal robustness*.

Suppose now the likelihood is gaussian in the data with covariance matrix $\boldsymbol{\Sigma}$ and expected means m_i . Then

$$\mathcal{L} = (2\pi)^{-N/2} |\boldsymbol{\Sigma}|^{-1/2} e^{-\frac{1}{2}\chi^2}, \quad (5)$$

where the χ^2 is defined as:

$$\chi^2 \equiv (\mathbf{x}_i - m_i)^t \boldsymbol{\Sigma}_{ij}^{-1} (\mathbf{x}_j - m_j). \quad (6)$$

The best-fit (minimum) χ^2 is then

$$\hat{\chi}^2 = (\mathbf{x}_i - \hat{m}_i)^t \boldsymbol{\Sigma}_{ij}^{-1} (\mathbf{x}_j - \hat{m}_j), \quad (7)$$

where \hat{m}_i are the best-fit means. The maximum of the likelihood is then:

$$\mathcal{L}_{\max} = (2\pi)^{-N/2} |\boldsymbol{\Sigma}|^{-1/2} e^{-\frac{1}{2}\hat{\chi}^2}, \quad (8)$$

so that we can rewrite Eq. (5) as

$$\mathcal{L} = \mathcal{L}_{\max} e^{-\frac{1}{2}(\chi^2 - \hat{\chi}^2)}. \quad (9)$$

According to (1), the N means m_i depend on n parameters

θ_k , i.e. $m_i = m_i(\theta)$.¹ The best-fit values \hat{m}_i are then functions of the best fit estimators $\hat{\theta}_k$, i.e. $\hat{m}_i = m_i(\hat{\theta})$. Here for simplicity we assume that Σ does not depend on the parameters, but this assumption can be easily lifted.

Let us assume now that the likelihood can be approximated near $\hat{\theta}$ by a Gaussian distributions also in the parameters, i.e.

$$\mathcal{L}(\mathbf{x}; \theta) \simeq f(\mathbf{x}; \theta) \equiv \mathcal{L}_{\max} e^{-\frac{1}{2}(\theta_i - \hat{\theta}_i)^t L_{ij} (\theta_j - \hat{\theta}_j)}, \quad (10)$$

where L_{ij} in the exponential factor is the inverse of the covariance matrix of the likelihood (or Fisher matrix, see e.g. Bassett et al. 2011; Amendola & Tsujikawa 2010) and where now the data are inside the best-fit estimators $\hat{\theta}_i$. Similarly, we assume a gaussian prior so that

$$\mathcal{P}(\theta_k) = \frac{|\mathbf{P}|^{1/2}}{(2\pi)^{n/2}} e^{-\frac{1}{2}(\theta_i - \tilde{\theta}_i)^t P_{ij} (\theta_j - \tilde{\theta}_j)}, \quad (11)$$

where $\tilde{\theta}_i$ are the prior means and \mathbf{P} is the prior matrix. It is now possible to evaluate the evidence analytically. Using the relation

$$\int d^n \mathbf{x} e^{-\frac{1}{2} \mathbf{x}^t \mathbf{A} \mathbf{x} + \mathbf{v}^t \mathbf{x}} = \frac{(2\pi)^{n/2}}{|\mathbf{A}|^{1/2}} e^{\frac{1}{2} \mathbf{v}^t \mathbf{A}^{-1} \mathbf{v}} \quad (12)$$

in

$$\begin{aligned} \mathcal{E} &= \int f(\mathbf{x}; \theta) \mathcal{P}(\theta) d^n \theta \\ &= \mathcal{L}_{\max} \frac{|\mathbf{P}|^{1/2}}{(2\pi)^{n/2}} \int \exp \left[-\frac{1}{2} (\theta_i - \hat{\theta}_i)^t L_{ij} (\theta_j - \hat{\theta}_j) \right. \\ &\quad \left. - \frac{1}{2} (\theta_i - \tilde{\theta}_i)^t P_{ij} (\theta_j - \tilde{\theta}_j) \right] d^n \theta, \end{aligned} \quad (13)$$

one finds

$$\mathcal{E} = \mathcal{L}_{\max} \frac{|\mathbf{P}|^{1/2}}{|\mathbf{F}|^{1/2}} e^{-\frac{1}{2}(\hat{\theta} - \tilde{\theta})^t \mathbf{L} \mathbf{F}^{-1} \mathbf{P}(\hat{\theta} - \tilde{\theta})}, \quad (14)$$

where $\mathbf{F} = \mathbf{P} + \mathbf{L}$. It will be convenient to rewrite the above equation as

$$\mathcal{E} = \mathcal{L}_{\max} \frac{|\mathbf{P}|^{1/2}}{|\mathbf{F}|^{1/2}} e^{-\frac{1}{2} \left(\hat{\theta}^t \mathbf{L} \hat{\theta} + \tilde{\theta}^t \mathbf{P} \tilde{\theta} - \theta'^t \mathbf{F} \theta' \right)}, \quad (15)$$

where $\theta' = \mathbf{F}^{-1}(\mathbf{L}\hat{\theta} + \mathbf{P}\tilde{\theta})$. In the limit in which the prior is very broad (so that $P_{ij} \ll L_{ij}$ and therefore $F_{ij} \rightarrow L_{ij}$) the argument of the exponential vanishes and we have simply

$$\mathcal{E} \simeq (2\pi)^{-N/2} e^{-\frac{1}{2} \hat{\chi}^2} \frac{|\mathbf{P}|^{1/2}}{|\mathbf{L}|^{1/2} |\Sigma|^{1/2}}. \quad (16)$$

2.2 Definition of internal robustness

Eq. (1) and its Fisher approximation Eq. (15) allow to compute the evidence \mathcal{E}_{tot} for a given cosmological model M_C and dataset d_{tot} . Suppose now that the data are actually coming from two completely different, and therefore independent, distributions. In other words, assume that a subset d_2 of d_{tot} actually depends on a totally different set of parameters (say, the properties of the SNIa progenitors or

galaxy environment), i.e., it is fully described by the systematic parameters of model M_S . Contrarily, the complementary set $d_1 = d_{\text{tot}} - d_2$ is still described by the cosmological parameters of model M_C . In this case the total evidence can be written as the product of the individual evidences:

$$\mathcal{E}_{\text{ind}} = \mathcal{E}_1 \mathcal{E}_2. \quad (17)$$

We can now use the Bayes ratio of Eq. (4) to quantify which hypothesis is favored. We thus compute²

$$\mathcal{B}_{\text{tot,ind}} = \frac{\mathcal{E}_{\text{tot}}}{\mathcal{E}_{\text{ind}}} = \frac{\mathcal{E}(\mathbf{x}; M_C)}{\mathcal{E}(\mathbf{x}_1; M_C) \mathcal{E}(\mathbf{x}_2; M_S)}, \quad (18)$$

and define

$$R \equiv \log \mathcal{B}_{\text{tot,ind}} \quad (19)$$

as the *internal robustness*. As discussed in the Introduction this quantity is related to the *external robustness* originally defined simply as *robustness* in March et al. 2011. The model M_S may be (and we will do so in the present paper) identified with the cosmological model M_C , see Section 2.4 for more details.

The previous equations give the general definition of internal robustness. It is however useful to evaluate analytically R in the Fisher approximation. Using Eq. (15) one finds:

$$\begin{aligned} \mathcal{B}_{\text{tot,ind}} &= \left(\frac{|\mathbf{L}_1 + \mathbf{P}_C| |\mathbf{L}_2 + \mathbf{P}_S|}{|\mathbf{L}_{\text{tot}} + \mathbf{P}_C| |\mathbf{P}_S|} \right)^{1/2} \frac{\mathcal{L}_{\max}^{\text{tot}}}{\mathcal{L}_{\max}^{[1]} \mathcal{L}_{\max}^{[2]}} \\ &\times e^{-\frac{1}{2} \left[\hat{\theta}_{\text{tot}}^t \mathbf{L}_{\text{tot}} \hat{\theta}_{\text{tot}} - \theta_{\text{tot}}'^t \mathbf{F}_{\text{tot}} \theta_{\text{tot}}' - \sum_i (\hat{\theta}_i^t \mathbf{L}_i \hat{\theta}_i - \theta_i'^t \mathbf{F}_i \theta_i') - \tilde{\theta}_2^t \mathbf{P}_S \tilde{\theta}_2 \right]} \\ &\simeq \left(\frac{|\mathbf{L}_1| |\mathbf{L}_2|}{|\mathbf{L}_{\text{tot}}| |\mathbf{P}_S|} \right)^{1/2} \left(\frac{|\Sigma_1| |\Sigma_2|}{|\Sigma_{\text{tot}}|} \right)^{1/2} e^{-\frac{1}{2} (\hat{\chi}_{\text{tot}}^2 - \hat{\chi}_1^2 - \hat{\chi}_2^2)}, \end{aligned} \quad (20)$$

where in the bottom line we simplified using Eq. (16), i.e., assuming the prior to be much broader than the likelihoods. Notice that the $(2\pi)^{-N/2}$ factors cancel out since $N_{\text{tot}} = N_1 + N_2$, where N_i is the size of the subset d_i . So far we have assumed gaussianity of the likelihoods, the existence of two independent distributions and the use of a very broad prior. If we make the additional assumption that the data points themselves are independent of one another (henceforth referred to as “raw data”), then the covariance matrix is diagonal, one has $|\Sigma_{\text{tot}}| = |\Sigma_1| |\Sigma_2|$ and we get the final formula for the internal robustness in the Fisher approximation:

$$R = R_0 + \frac{1}{2} \log \left(\frac{|\mathbf{L}_1| |\mathbf{L}_2|}{|\mathbf{L}_{\text{tot}}|} \right) - \frac{1}{2} (\hat{\chi}_{\text{tot}}^2 - \hat{\chi}_1^2 - \hat{\chi}_2^2), \quad (21)$$

where R_0 is a constant coming from the unknown determinant of the systematic prior, $R_0 = -\frac{1}{2} \log |\mathbf{P}_S|$.

The first factor in Eq. (21), formed out of the determinants, expresses Occam’s razor factor of parameter volumes, while the second penalizes R if the two probes are very different from each other (so the hypothesis that they come from different models, or equivalently that systematics are important, is favored). We expect, therefore, the internal robustness to be a measure of how much subsets of a dataset

¹ Note that to simplify the notation we will drop in the following equations the superscript M of the model in question.

² It is straightforward to generalize Eq. (18) to more than two partitions such that $\mathcal{E}_{\text{ind}} = \mathcal{E}_1 \mathcal{E}_2 \mathcal{E}_3 \dots$

overlap: the more they do, the more compatible the two datasets are.

In order to help intuition, we can evaluate R for the simplified case in which *a)* we can neglect the logarithmic part; *b)* there is only one parameter; *c)* the errors are all identical ($\sigma_i = \sigma$); and *d)* the subset d_2 consists of a single point x_2 . Then we have $\hat{\chi}_2^2 = 0$ and for $N_1 \simeq N_{\text{tot}} \gg 1$

$$R \approx -\frac{1}{2} \frac{(x_2 - \hat{m}_{\text{tot}})^2}{\sigma^2} \quad (22)$$

i.e. R reduces to the scatter of x_2 from the best fit \hat{m}_{tot} evaluated by fitting the remaining N_1 elements. Therefore a large and negative R means x_2 is an outlier.

2.3 Statistical properties of internal robustness

In order to understand the statistical properties of the internal robustness let us start by fixing the subset d_2 to some d_2^* (d_1^* is just the complementary subset). Let us also assume that data come from the cosmological model M_C only. From Eq. (21) we can then calculate the probability distribution function of $R(d_2^*)$ (denoted as eR-PDF). If one also neglects the logarithmic term (Occam's razor factor), then (in this very particular case) R becomes the parameter goodness-of-fit test introduced by [Maltoni et al. 2002](#), and it was shown by [Maltoni & Schwetz 2003](#) that $R(d_2^*)$ is distributed as a χ^2 distribution with n_{tot} degrees of freedom (d.o.f.). The full eR-PDF is then a modified χ^2 distribution with n_{tot} d.o.f., not too distorted as Occam's razor factor is logarithmically suppressed. If we now drop the assumption that data come from the cosmological model M_C , we can use the (fiducial) eR-PDF to assess the significance of a given value of $R(d_2^*)$, for example of a low value that could indicate that the dataset is systematics driven. We remind indeed the reader that in our fully Bayesian context the robustness R is related to the Bayes ratio of the evidences and a small (large) R disfavors (favors) the description of the dataset by the cosmological model M_C alone.

As far as the internal robustness is concerned, however, we do not intend to fix d_2 to a particular subset (even if we may still do so if useful). The above way of proceeding is suited indeed to the external robustness, the aim of which is to analyze two different datasets (e.g. CMB and BAO). The idea behind the internal robustness is instead to keep the total dataset fixed (i.e. not to be concerned with the statistical distribution of $R(d_{\text{tot}})$) and evaluate $R(d_2)$ for all the possible partitions of d_{tot} , thus generating a distribution which we call iR-PDF. Internal and external robustness have therefore very *different* statistical properties.

The fiducial iR-PDF (assuming that data come from the cosmological model M_C only) is a highly nontrivial object. Even if one neglects Occam's razor factor, it is *not* a χ^2 distribution with n_{tot} d.o.f., as the sampling of d_2 is constrained within a fixed realization of d_{tot} , on which the iR-PDF depends. As a simple example of the difference between the latter two distributions, the iR-PDF has a compact and discrete support as it is sampled over a finite number of subsets. We will see in Section 4.1.4, however, that for the datasets treated in this paper the binned iR-PDF (neglecting Occam's razor factor) is rather close to a χ^2 distribution with n_{tot} degrees of freedom.

The iR-PDF gives the probability that a given value

of R is realized among the available subsets. However, differently from the eR-PDF, the iR-PDF cannot be used to assess the significance of a given value of R . To do so, we need to compute a distribution of iR-PDFs, which we will obtain by evaluating the robustness in many Montecarlo realizations of mock catalogues. We would like to stress that thanks to this approach our analysis will not be affected by the possible Bayesian penalization of models with many parameters.

2.4 Systematic parameters

Generally speaking, there are two possible choices for the parameters for the subset d_2 . In the first case, which we will adopt in the analysis of this paper, the parametrization is analog to the cosmological one, e.g. $\{\Omega_{m0}, \Omega_{\Lambda0}, \alpha\}$, where $\Omega_{m0}, \Omega_{\Lambda0}$ are the present-day matter and dark-energy parameters and α is combination of the unknown magnitude offset M_0 (sum of the SNe absolute magnitudes, of k -corrections and other possible systematics) and the Hubble parameter H_0 : $\alpha \equiv M_0 - 5 \log_{10} H_0 / 10 \text{pc}$ ([Amendola & Tsujikawa 2010](#)). In this case $\mathbf{P}_S = \mathbf{P}_C$. This would be the preferred choice if we expect some of the SNe to be better described by different cosmological parameters. For instance the parameters could differ in different line-of-sight directions (say, 3 different Hubble parameters H_{x0}, H_{y0} and H_{z0} , as in anisotropic models with shear, see [Graham et al. 2010; Colin et al. 2011](#)) or in different redshift shells (say, Ω_{m0}^{in} and Ω_{m0}^{out} as in some inhomogeneous models, see [Garcia-Bellido & Haugboelle 2008; Marra & Notari 2011; Jackson 2012](#)). We could also erroneously interpret the unknown systematic parameters as the cosmological ones and therefore employ the same parameter names and the same prior function.

In the second case, not to be explored here, one could choose a completely phenomenological parametrization such as

$$m(z) = \sum_{i=0}^j \lambda_i f_i(z) \quad (23)$$

for the theoretical magnitudes. Here the functions $f(z)$ could be arbitrarily chosen, e.g. $f_i(z) = z^i$. If $j = 2$ we have then $m = \lambda_0 + \lambda_1 z + \lambda_2 z^2$. Since the λ 's are linear parameters, both best fit and Fisher matrix would be analytical. This second choice would be appropriate if one expects some of the SNe to be dominated by systematic effects unrelated to cosmology, say because of sample contamination or strong environmental effects.

Restricting ourselves to the first case, we can marginalize over α analytically ([Amendola & Tsujikawa 2010](#)). Let us define the sums (remember that the covariance matrix Σ is diagonal)

$$S_n = \sum_{i=1}^{N'} \frac{M_i^n}{\sigma_i^2}, \quad (24)$$

where $N' = N_{1,2}$, $M_i \equiv x_i - m_i = x_i - 5 \log_{10} \bar{d}_L(z_i)$, $\bar{d}_L = d_L H_0$ and d_L is the luminosity distance. Marginalizing over

the constant offset α we obtain

$$-\log \mathcal{L} = \frac{1}{2} \chi_{\text{mar}}^2 + \frac{1}{2} \log \frac{S_0}{2\pi} + \sum_{i=1}^{N'} \log(\sqrt{2\pi} \sigma_i), \quad (25)$$

where

$$\chi_{\text{mar}}^2 = S_2 - \frac{S_1^2}{S_0}. \quad (26)$$

As the likelihood is gaussian in the data, minimizing the marginalized χ_{mar}^2 with respect to $\{\Omega_{m0}, \Omega_{\Lambda0}\}$ gives the same result as minimizing the original χ^2 with respect to $\{\Omega_{m0}, \Omega_{\Lambda0}, \alpha\}$. Therefore, even though we are in a Bayesian context, $\hat{\chi}_{\text{mar}}^2$ is still distributed as a χ^2 with $N' - 3$ degrees of freedom. Note also that if the original, non-marginalized data is independent, then so will be the data marginalized over α . To see this, one can rewrite the marginalized likelihood as

$$\mathcal{L} \propto \exp \left[-\frac{1}{2} (\mathbf{x} - \mathbf{m})^t \bar{\Sigma}^{-1} (\mathbf{x} - \mathbf{m}) \right], \quad (27)$$

where $\bar{\Sigma}^{-1} = \Sigma^{-1} - \Sigma^{-2}/S_0$, which for a diagonal Σ is still a diagonal matrix.

Recalling that in general a Fisher matrix is given by

$$L_{pq} = -\frac{\partial^2 \log \mathcal{L}}{\partial \theta_p \partial \theta_q}, \quad (28)$$

we get for the cosmological Fisher matrices \mathbf{L}_{tot} , \mathbf{L}_1 and \mathbf{L}_2 the general expression

$$\begin{aligned} L_{pq} &= \frac{1}{2} S_{2,pq} - \frac{1}{S_0} (S_1 S_{1,pq} + S_{1,p} S_{1,q}) \\ &= \sum_i \frac{M_{i,pq}}{\sigma_i^2} \left(M_i - \frac{S_1}{S_0} \right) + \sum_i \frac{M_{i,p} M_{i,q}}{\sigma_i^2} \\ &\quad - \frac{1}{S_0} \sum_i \frac{M_{i,p}}{\sigma_i^2} \sum_j \frac{M_{j,q}}{\sigma_j^2} \\ &= \frac{5}{\ln 10} \sum_i \frac{1}{\sigma_i^2} \left[\frac{\bar{d}_{Li,p} \bar{d}_{Li,q}}{\bar{d}_{Li}^2} - \frac{\bar{d}_{Li,pq}}{\bar{d}_{Li}} \right] \left(M_i - \frac{S_1}{S_0} \right) \\ &\quad + \left[\frac{5}{\ln 10} \right]^2 \left[\sum_i \frac{\bar{d}_{Li,p} \bar{d}_{Li,q}}{\sigma_i^2 \bar{d}_{Li}^2} - \frac{1}{S_0} \sum_i \frac{\bar{d}_{Li,p}}{\sigma_i^2 \bar{d}_{Li}} \sum_j \frac{\bar{d}_{Lj,q}}{\sigma_j^2 \bar{d}_{Lj}} \right]. \end{aligned} \quad (29)$$

Finally, the robustness in the Fisher approximation is given in this case [see Eq. (25)] by:

$$\begin{aligned} R &= R_0 - \frac{1}{2} \log(2\pi) \\ &\quad + \frac{1}{2} \log \left(\frac{S_{0,1} S_{0,2} |\mathbf{L}_1| |\mathbf{L}_2|}{S_{0,\text{tot}} |\mathbf{L}_{\text{tot}}|} \right) - \frac{1}{2} (\hat{\chi}_{\text{tot}}^2 - \hat{\chi}_1^2 - \hat{\chi}_2^2). \end{aligned} \quad (30)$$

Note that in the following results we will express the numerical values of the robustness as $R - R_0 - \log(2\pi)$, to which we will refer simply as R .

In Section 4 we shall use supernova data provided by the Union2.1 (Suzuki et al. 2012) collaboration in the form of a 3-column matrix, each row $\{z_i, x_i, \sigma_i\}$ consisting of redshift z_i , distance modulus x_i and distance modulus error σ_i . This matrix was computed using the SALT2 method (Guy et al. 2007), and the nuisance parameters α and β controlling stretch and color corrections were fixed to the best-fit values (to wit $\alpha = 0.1219$, $\beta = 2.466$). Used in this way, the supernova data are rigorously not independent, as the values of the distance moduli are obtained after processing

the raw data assuming a particular cosmological model (see, e.g. Marriner et al. 2011). As in this first work we mainly aim at presenting the method, we will ignore however such correlations.³ Note, however, that if on one hand this is a caveat for the results that follow, on the other hand it presents an opportunity to cross-check the Union2.1 data (often naively employed in such concise form) for leftover systematics.

3 SCANNING THE SUBSETS

In order to obtain the full iR-PDF we have to compute $\hat{\chi}_{1,2}^2$ and $\mathbf{L}_{1,2}$ for every partition $d_{1,2}$ of a given dataset of N_{tot} elements. There are

$$2^{N_{\text{tot}}-1} - 1 \approx 10^{0.3 N_{\text{tot}}} \quad (31)$$

possible partitions and we find that in the present application a complete scan of all subsets is unfeasible for $N_{\text{tot}} \gtrsim 20$. The issue then arises of which subset Ξ among all possible partitions to form. We extract from the entire Union2.1 catalogue a number T of subsets d_2 composed by a number N_2 of SNe between $N_{2,\text{min}}$ and $N_{2,\text{max}}$ chosen at random among all the possible combinations. However, a pure random sampling (i.e. uniform in the space of all possible partitions) would pick with extremely high probability only the most populated subsets (in our case with $N_2 \sim N_{2,\text{max}}$). Since we would like to explore also the smaller subsets, we adjust the selection so as to obtain a distribution approximately uniform in N_2 (i.e. approximately equal number of subsets for every value of N_2). We call this particular set $\Xi(T)$, and the following analysis depends on it. In particular T gives the statistics of the analysis, while the definition of Ξ determines the way the sets have been chosen. We will consider different strategies in forthcoming work.

The upper limit we use is $N_{2,\text{max}} = N_{\text{tot}}/2$. This is due to the fact that, as we are using the cosmological parametrization, the robustness is symmetric in the datasets d_1, d_2 so that scanning half of the catalogue is enough. In order to discuss $N_{2,\text{min}}$ it is important to stress that we consider a much larger parameter space than the usual physical one, as Ω_{m0} and $\Omega_{\Lambda0}$ also parametrize the (possibly cosmology unrelated) systematic parameters. The range we adopt is $-10 < \Omega_{m0} < 10$ and $-20 < \Omega_{\Lambda0} < 10$, and we exclude the $\{\Omega_{m0}, \Omega_{\Lambda0}\}$ region of the parameter space for which the expansion rate $H(z)$ is negative for $z < 2$, which well accommodates the redshift range of the Union2.1 dataset. This is a relaxation of the usual no-big-bang excluded region, see Appendix A for more details. The value of $N_{2,\text{min}}$ is then found by demanding that the likelihood of the smaller subset d_2 has support within the parameter space considered. We have found empirically that a value of $N_{2,\text{min}} = 10$ satisfies on average this requirement.

We will now explain how we actually computed the robustness. For subsets with N_2 larger than a certain $N_{2,\text{med}}$ we have found that the likelihood can be adequately represented by a Gaussian distribution in the parameter space, so as to legitimate the Fisher approach. The advantage of using the Fisher matrix is in the computational speed gain, as

³ It is worth stressing that the important factor is the independence of the data points, not of their error bars, which even if completely correlated would not affect the results.

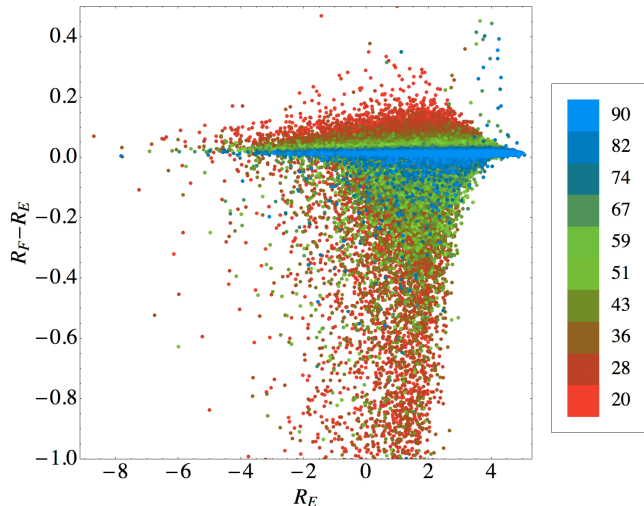


Figure 1. Comparison between the exact robustness R_E and its Fisher approximation R_F for a random set of subsets. Each subset is represented by a point, which is color coded according to the corresponding number N_2 of SNe in the subset d_2 . This analysis clearly shows that, as far as the robustness is concerned, the Fisher approximation holds better for larger subset sizes. See Section 3 for more details.

only the maximum of the likelihood and few derivatives have to be found numerically. For smaller subsets $N_2 \leq N_{2,\text{med}}$, however, the likelihood deviates from a Gaussian distribution and we are forced to integrate the likelihood numerically over the full parameter space. In order to empirically find $N_{2,\text{med}}$ we have computed both the exact robustness R_E of Eq. (18) and its Fisher approximation R_F of Eq. (21) for a random set of subsets. Fig. 1 shows how the discrepancy decreases as the subset d_2 becomes larger. As we will see below in Fig. 4, the iR-PDF varies on a scale of order unity in robustness. Therefore, we want to keep the error in the robustness computation at a level $\lesssim 0.1$. We found that the value $N_{2,\text{med}} = 90$ satisfies this requirement.

4 RESULTS

In analyzing the Union2.1 catalogue of 580 SNe we will restrict to the case of the curved Λ CDM model, i.e., we allow for spatial curvature but fix the equation of state parameter ($w = -1$). The cosmological parameters are therefore the present-day density parameters Ω_{m0} and $\Omega_{\Lambda0}$, with the addition of the nuisance offset α . We will consider other parameterizations in forthcoming work.

Our results will be divided into three parts. First in Section 4.1 we will test our method with a mock dataset whose SNe were drawn from two very different cosmological models. In Section 4.2 we will analyze the Union2.1 dataset (Suzuki et al. 2012) including previously-excluded supernovae (i.e., SNIa that did not pass all the quality selection cuts); this also should be a test for our method. Finally, in Section 4.3 we will present our results regarding the actual Union2.1 dataset.

Before dealing with our results, it is useful to define what we mean by “mock catalogue”. A mock catalogue \mathcal{M} for a given dataset \mathcal{D} is a synthetic unbiased

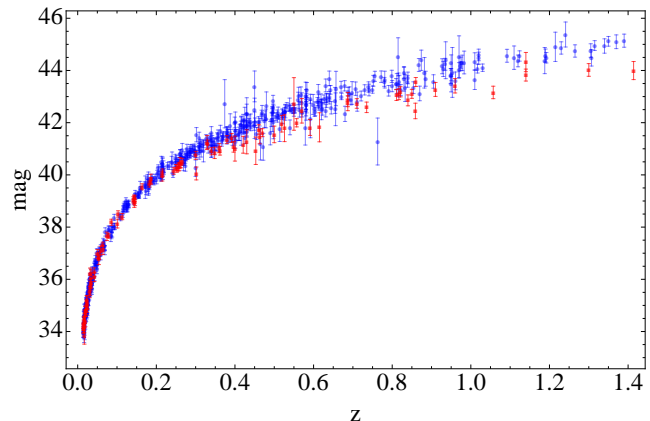


Figure 2. Plotted is the distance modulus of the SNe of the systematics-driven dataset \mathcal{D}_{EdS} in which 100 SNe have been drawn from the EdS model as fiducial model (red data) and the remaining from the best-fit model of Union 2.1 (blue data). Without the different coloring it would be difficult to spot by eye the EdS SNe (the challenged reader could try it on a B&W printer). See Section 4.1.1 for more details.

dataset generated using the best-fit model of \mathcal{D} as the fiducial model. More precisely, we keep fixed the redshifts z_i and errors σ_i of \mathcal{D} , and change the distance moduli to $x_{\text{mock}} = m_{\text{fiducial}} + x_{\text{random}}$ where x_{random} is drawn from a gaussian distribution of zero mean and standard deviation σ_i .

4.1 Systematics-driven dataset

4.1.1 Dataset and iR-PDF computation

In order to test our method we have generated a systematics-driven dataset \mathcal{D}_{EdS} in the following way. First we have created a mock catalogue of Union2.1. Then we replaced 100 randomly chosen distance-modulus entries with others drawn taking the Einstein-de Sitter (EdS) model (flat, matter-dominated) as the fiducial one (instead of the best-fit model of Union2.1). These 100 SNe are shown in red in Fig. 2. One expects for \mathcal{D}_{EdS} very low robustness values, as for the subset of 100 EdS SNe it is clearly favored the possibility that d_1 and d_2 have independent cosmological parameters (which, we remind, we use to parametrize also the systematics). In the case of d_2 being exactly the subset of 100 EdS SNe, one obtains the plot of Fig. 3 which shows the 1, 2 and 3 σ confidence-level contours for d_{tot} and d_1, d_2 independently. The contours are indeed far apart and the robustness is extremely low, $R_{\text{min}} \simeq -97.5$ (as previously mentioned, we know *a posteriori* that R is typically a $\mathcal{O}(1)$ quantity). Fig. 3 summarizes nicely the ultimate goal of internal robustness, that is, to go from the original set in green to the “decontaminated” set in red. The contours do not look significantly different (i.e. same precision), but their position has substantially moved by $\sim 3\sigma$ (i.e. much better accuracy).

We will now pretend that \mathcal{D}_{EdS} is made of real data and test the sensitivity of our method with it. Before proceeding, however, one can see that the dataset is sick by means of the standard goodness-of-fit test given by $\bar{\chi}^2 = \hat{\chi}^2 / (N_{\text{tot}} - 3)$ (the cosmological model has three parameters). For \mathcal{D}_{EdS} we

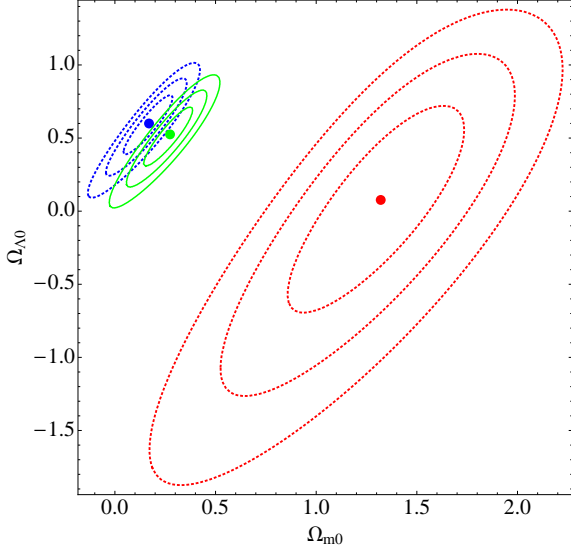


Figure 3. 1, 2 and 3σ confidence-level contours for subsets d_1 (blue) and d_2 (red), where d_2 is made of the 100 systematics-driven EdS SNe shown in red in Fig. 2. The contours are far apart and the robustness is indeed extremely low, $R \simeq -97.6$. Also shown in green are the confidence-level contours for the complete dataset d_{tot} . The 100 EdS SNe clearly bias the likelihood surface of the full dataset. See Section 4.1.1 for more details.

find indeed $\bar{\chi}^2 = 1.39$, that is, the catalogue is incompatible with the theoretical model at $6\text{-}\sigma$ level. Nevertheless we advocate that internal robustness is a better test than the standard goodness-of-fit; in other words we would like to show that we can give a stronger exclusion. In order to do so, we will “normalize” \mathcal{D}_{EdS} by adding a constant $\sigma_{\text{int}}^{\text{extra}}$ to the errors σ_i such that $\bar{\chi}^2 = 1$. This procedure should favor the single cosmological model M_C as the normalized catalogue passes the goodness-of-fit test; the idea is to see if the internal-robustness test can still show that the dataset is systematics driven.

The technique of normalizing a catalogue to $\bar{\chi}^2 = 1$ is actually often used in supernova cosmology (Astier et al. 2006). SNe are indeed imperfect standard candles with a residual scatter, called the intrinsic dispersion, of roughly $\sigma_{\text{int}} \sim 0.1$ magnitudes. As SN physics is not yet thoroughly understood, σ_{int} is not tightly constrained, and it is often determined by demanding that $\bar{\chi}^2 = 1$.⁴ SNe catalogues are therefore perfect candidates for testing the internal robustness method. Since the Union2.1 data already include implicitly a σ_{int} , what we call $\sigma_{\text{int}}^{\text{extra}}$ is the amount to be added to σ_{int} in order to have $\bar{\chi}^2 = 1$. For \mathcal{D}_{EdS} one needs $\sigma_{\text{int}}^{\text{extra}} = 0.0356$ magnitudes; that is, to increase the errors. As a consequence the contours of Fig. 3 become slightly broader and the minimum robustness is larger, even though still extremely low: $R_{\text{min}} \simeq -70.9$.

Finally, we computed the internal robustness for the (normalized) \mathcal{D}_{EdS} dataset using the set of partitions $\Xi(T)$

with a statistics of $T = 5 \cdot 10^5$ subsets (see Section 3). As explained in Section 2.3, in order to determine if the iR-PDF of \mathcal{D}_{EdS} passes or not the robustness test, we have to generate a distribution of iR-PDFs, which we obtain by computing the internal robustness for 100 mocks \mathcal{M}_j . Each mock iR-PDF is generated using the same set prescription $\Xi(T)$ but with a lower statistics of $T = 5 \cdot 10^4$, as the fluctuations among the mocks are more important than the “sampling” fluctuations due to poissonian errors. The mock catalogues \mathcal{M}_j have been also normalized to $\bar{\chi}^2 = 1$. It is worth saying at this point that the robustness test is quite expensive from a computational point of view. The numerical results of this paper have been obtained with Wolfram Mathematica 8 and the average CPU time to calculate the robustness value of a given partition was $\sim 2 - 3$ seconds (luckily the computation is easily parallelized). The size of T and the number of mocks used are therefore the main constraints in the final results: the higher the statistics, the clearer the signal one may get.

4.1.2 Analysis of the iR-PDF

The left panel of Fig. 4 shows the iR-PDF of \mathcal{D}_{EdS} (solid orange line), which has been obtained by binning the robustness values within N_b bins of widths ΔR_k . The same binning prescription has been used to calculate also the bin heights h_{kj} of the unbiased mocks \mathcal{M}_j , which have been used to compute mean \bar{h}_k and standard deviation σ_{h_k} for the N_b bins. By assuming that the bin heights within a given bin are distributed according to a gaussian PDF with mean \bar{h}_k and the standard deviation σ_{h_k} , we have then drawn the σ -bands bounding a systematics-free iR-PDF (gray areas in the left panel of Fig. 4). From this plot it seems as if the iR-PDF of \mathcal{D}_{EdS} passes the internal robustness test.

One expects, however, the signal to be concentrated in the low-robustness tail of the PDF, in which systematics-driven SNe should dominate one of the two partitions $d_{1,2}$. The spurious iR-PDF can indeed be loosely thought as the sum of a systematics-free PDF and a systematics-driven perturbation. The systematics-free PDF will behave according to the σ -bands, which do not change sizably if the biased subset is sufficiently small. The perturbation will then be given by the 100 EdS SNe which, when d_2 coincides with them, will add a *single* point to the histogram at $R_{\text{min}} \simeq -70.9$. This point is clearly not observable in practice as one cannot scan all the 10^{174} possible subsets. At the expense of a higher robustness, however, there will be many subsets d_2 with a fraction of the 100 EdS SNe, thus generating a stronger low-robustness tail in a biased dataset.

In order to analyze the low-robustness tail of the PDF, we have to drop the gaussian assumption. The latter is indeed a good approximation only for the bins in the body for which $\bar{h}_k/\sigma_{h_k} \gg 1$, but not in the tail as illustrated in Fig. 5 where the distributions for two low-robustness bins are shown. The reason is that the iR-PDFs of the mocks have a compact support which have a variable R_{min} . At a given low value R in the tail, therefore, some of the robustness distributions of the mocks will be very close (if not identical) to zero, with the consequence that the distribution of the bin heights will be skewed, thus deviating from gaussianity. Note that this cannot be cured by using a higher statistics

⁴ Note that this procedure may hide problems with the theoretical model being used, as it is shown by the very example of \mathcal{D}_{EdS} . For further discussion and alternatives see Kim 2011; March et al. 2011; Lago et al. 2011.

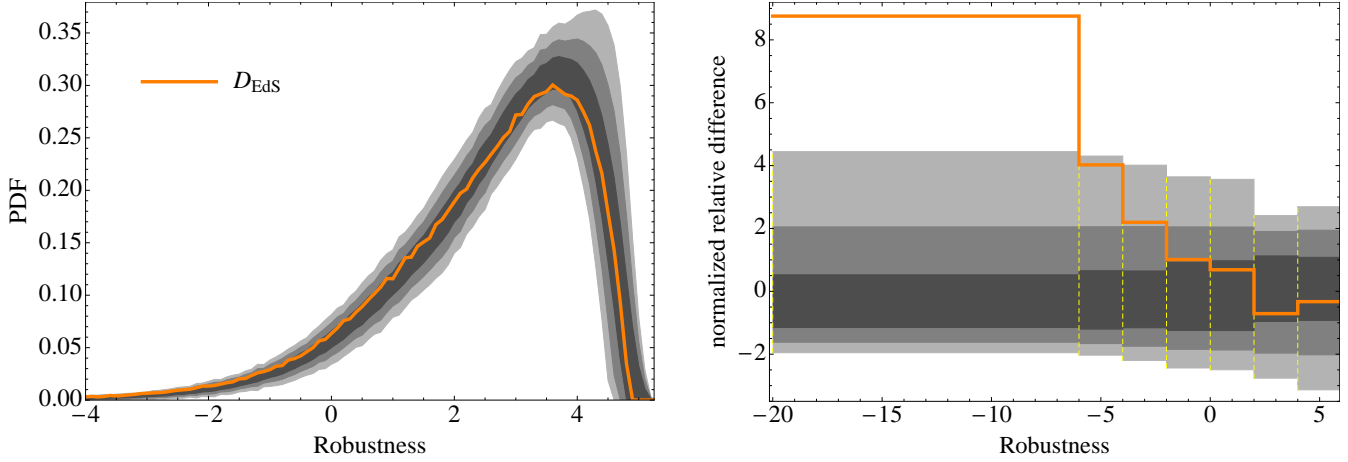


Figure 4. [Left]: binned internal-robustness PDF (orange curve) for the dataset \mathcal{D}_{EdS} of Fig. 2 against σ -bands (gray areas) from (unbiased) mock catalogues. [Right]: same as the left panel for larger bins (dashed lines) and lower robustness values. Moreover, the bin height values h_k have been translated and scaled according to $h_k \rightarrow (h_k - \bar{h}_k)/\sigma_{h_k}$ in order to uniformly show the signal across the various bins. One can clearly see that while the body of the iR-PDF is compatible with the mocks, the low-robustness tail is detected as being driven by systematics. The \mathcal{D}_{EdS} datum relative to the bin $(-20, -6]$ lies at 4.2σ confidence levels. See Section 4.1.2 for more details.

T as this feature is related to the existence of an R_{\min} for the iR-PDF.

In order to analyze the tail, the standard way to proceed would be to generate many mock iR-PDFs so as to compute the non-gaussian distribution in the bin heights numerically. As remarked earlier, however, it is numerically expensive to obtain an iR-PDF and we limit our sample of mock catalogues to 100. In order to properly quantify the signal we have then proceeded in two ways. The first and most obvious is to check if any mock has a bin height larger than \mathcal{D}_{EdS} . As shown by Fig. 5 this is not the case for the lowest bin (where we expect the signal to be strongest), and we can so conclude that \mathcal{D}_{EdS} is systematics-driven at a confidence level better than 99%, or 2.6σ .

The second way is to use a template to be fitted to the data, and then use the fitted template to assess the significance of the datum relative to \mathcal{D}_{EdS} . We used as template the Pearson distribution (Pearson 1895, 1916), which is found by demanding that its first four moments coincide with the moments from the bin heights. The result is depicted by a solid black in Fig. 5, where also the gaussian distribution is plotted for comparison. As one can see the fitted Pearson distribution correctly reproduces the skewness of the data, and in particular does not go to negative bin height, as instead does the gaussian distribution for the lowest bin.

Having calculated the σ -levels with the Pearson template, we can now show our final results in the right panel of Fig. 4. We have used larger bins as compared to the plot in the left panel because the bins extend to lower robustness values, which have lower statistics. Also, the bin height values h_k have been translated and scaled according to:

$$h_k \rightarrow \frac{h_k - \bar{h}_k}{\sigma_{h_k}}, \quad (32)$$

so as to uniformly show the signal across the various bins. Fig. 4 clearly shows how the body of the iR-PDF of \mathcal{D}_{EdS} passes the robustness test, as opposed to the low-robustness

tail which is detected as being systematics-driven. More precisely, the \mathcal{D}_{EdS} datum relative to the bin $(-20, -6]$ lies at 4.2σ confidence levels, while the datum relative to the robustness bin $(-6, -4]$ lies at 2.8σ confidence levels. Note that in the previous results we did not include the error in the datum relative to \mathcal{D}_{EdS} . The latter is indeed negligible as the iR-PDF of \mathcal{D}_{EdS} has been found with a statistics much higher than the one relative to the iR-PDF of the mocks.

Finally, one would expect non-negligible fluctuations in the third (skewness) and forth (kurtosis) moments coming from a sample of only 100 data, and in order to assess the uncertainty on the exclusion signal, one may proceed as follows. Repeat enough times: a) generate 100 random values from the fitted Pearson PDF; b) fit again the Pearson PDF to this new data and calculate the σ confidence level. If we now apply this routine to the two lowest bins of Fig. 5 for which the signal is 4.2σ and 2.8σ , respectively, we find that the signal is $> 3.3\sigma$ and $> 2.3\sigma$ at 95% confidence level, respectively.

4.1.3 Taking correlations into account

When interpreting the results in Fig. 4 one cannot neglect the correlations among the bins ΔR_k . In other words, to get a reliable estimate by eye one is supposed to consider only one bin at a time (namely the bin with the strongest signal) and is not allowed to combine the signals from various bins as (all) the bins are most likely correlated. The same procedure can also be followed numerically to get the simplest conservative estimate (see previous Section).

As the signal is concentrated in the low-robustness tail, where the gaussian assumption is not a good approximation, we compute the correlation by building a histogram. In Fig. 6 we show the corresponding contour plot for the two lowest-robustness bins together with the corresponding datum of \mathcal{D}_{EdS} (orange disk). As with only 100 mocks it is not possible to obtain a good enough PDF which can then be in-

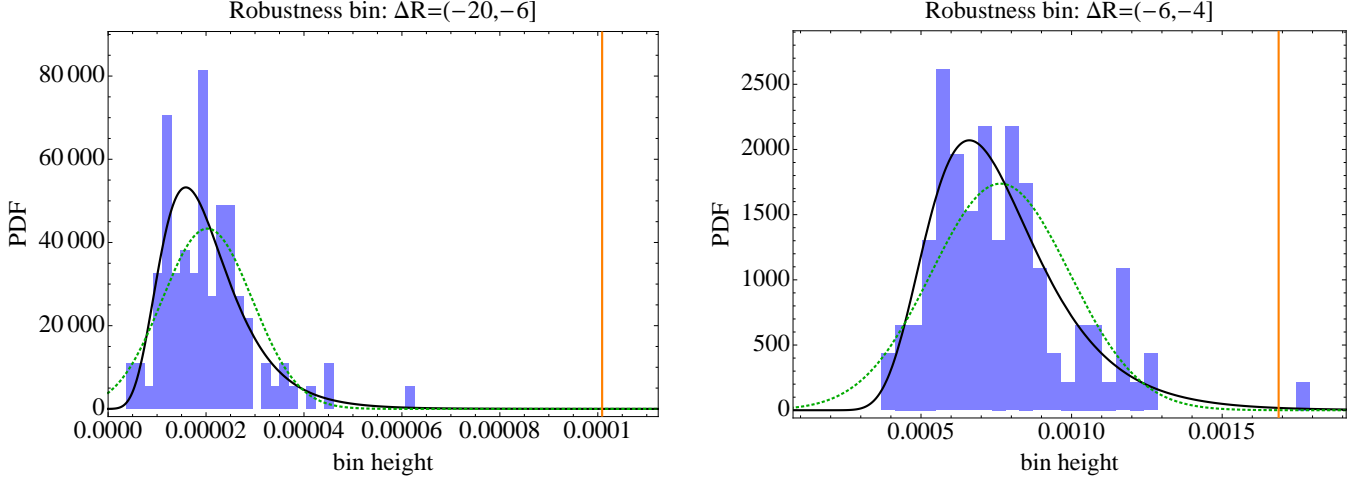


Figure 5. Binned distributions of bin heights for the lowest (left panel) and next-to-lowest (right panel) robustness bins of the mock robustness distributions used to make the σ -bands shown on the right panel of Fig. 4. The bin height corresponding to \mathcal{D}_{EdS} is shown as an orange vertical line, and corresponds to the orange curve on the right panel of Fig. 4. The dotted line is a fitted gaussian distribution. The solid line is the fitted Pearson distribution which has been used to draw the σ -bands shown on the right panel of Fig. 4. See Section 4.1.2 for more details.

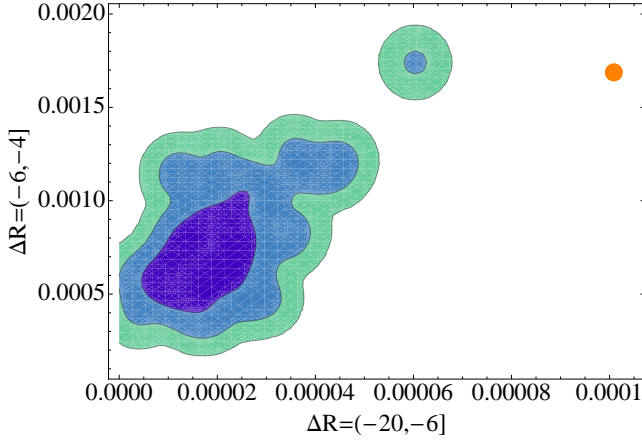


Figure 6. Correlated distribution of bin heights for the two lowest-robustness bins of Fig. 5. The 1, 2 and 3σ confidence-level contours have been calculated using the gaussian values $\Delta\chi^2 = 2.30, 6.17, 11.8$. The bin height corresponding to \mathcal{D}_{EdS} is shown as an orange disk. See Section 4.1.3 for details.

egrated to calculate the contours, in Fig. 6 the contours are drawn using gaussian values, to wit: $\Delta\chi^2 = 2.30, 6.17, 11.8$. From this analysis it looks as if taking correlations into consideration would increase the signal.

4.1.4 Frequentist limit

If one neglects the logarithmic part in Eq. (30), then the robustness for the unbiased mocks becomes the parameter goodness-of-fit test (Maltoni et al. 2002; Maltoni & Schwetz 2003) which is distributed as a χ^2 distribution with 3 degrees of freedom. As explained in Section 2.3, however, this is exactly true only for the external robustness, but not for the internal robustness. Nevertheless, the χ^2 distribution with 3 d.o.f. captures the overall behavior of a fiducial iR-PDF, as

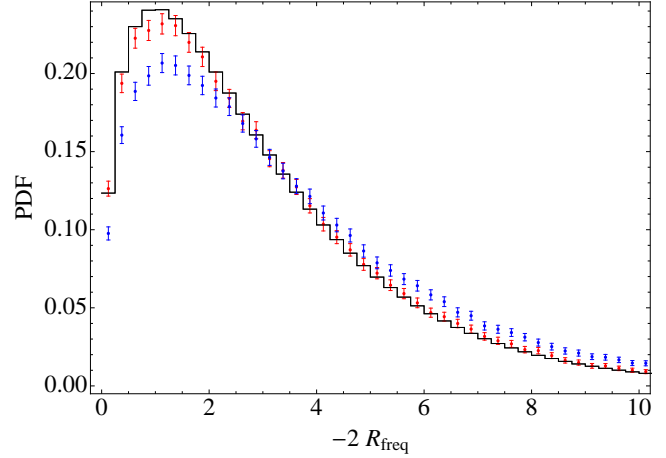


Figure 7. Binned iR-PDF using for the robustness its frequentist limit $-2R_{\text{freq}} \equiv \hat{\chi}_{\text{tot}}^2 - \hat{\chi}_1^2 - \hat{\chi}_2^2$. Distributions relative to two unbiased mock catalogues are shown in red and blue, while the binned χ^2 distribution with 3 d.o.f. is shown with a black curve. The error bars stand for 3σ . It is clear that the χ^2 distribution with 3 d.o.f. is not the correct PDF even though it captures the overall shape. See Section 4.1.4 for more details.

can be seen in Fig. 7 where is plotted the quantity

$$R_{\text{freq}} \equiv -\frac{1}{2} (\hat{\chi}_{\text{tot}}^2 - \hat{\chi}_1^2 - \hat{\chi}_2^2) \quad (33)$$

for two mock catalogues (red and blue) together with the binned χ^2 distribution with 3 d.o.f. (black). Note that when the best fits of d_1 and d_2 coincide one has $R_{\text{freq}} = 0$.

4.2 Union2.1 dataset with previously-excluded SNe

To further test our systematic search for systematic biases, it would be interesting to apply the internal robustness method

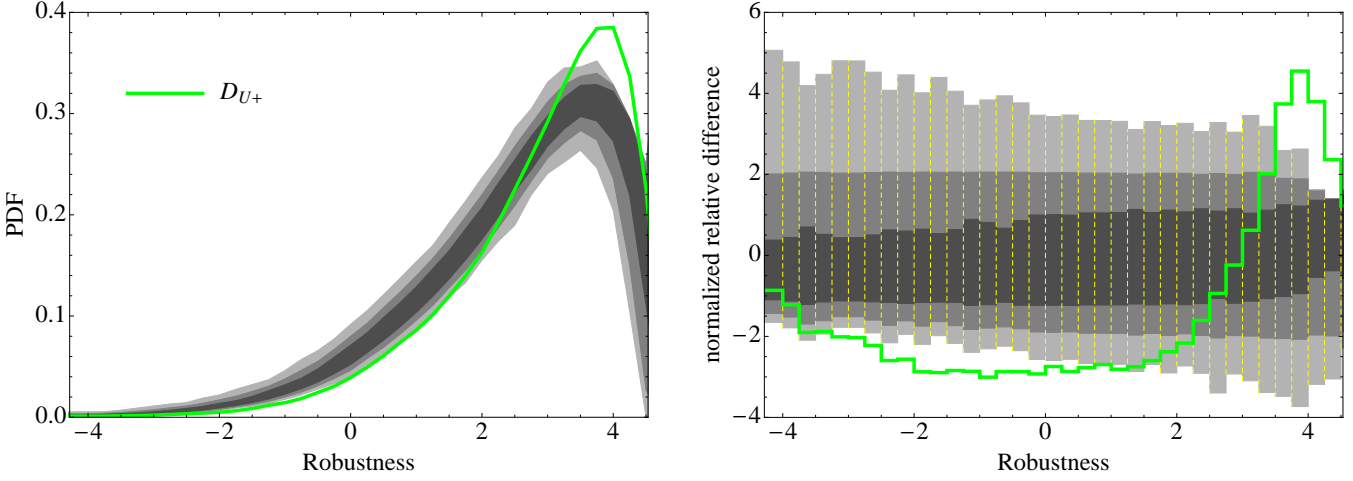


Figure 9. Same as Fig. 4 for the dataset \mathcal{D}_{U+} of Fig. 8 (green curve). One can clearly see that in this case the (strong) signal of \mathcal{D}_{U+} as being systematics-driven comes from the bins in the body of the PDF. See Section 4.2 for more details.

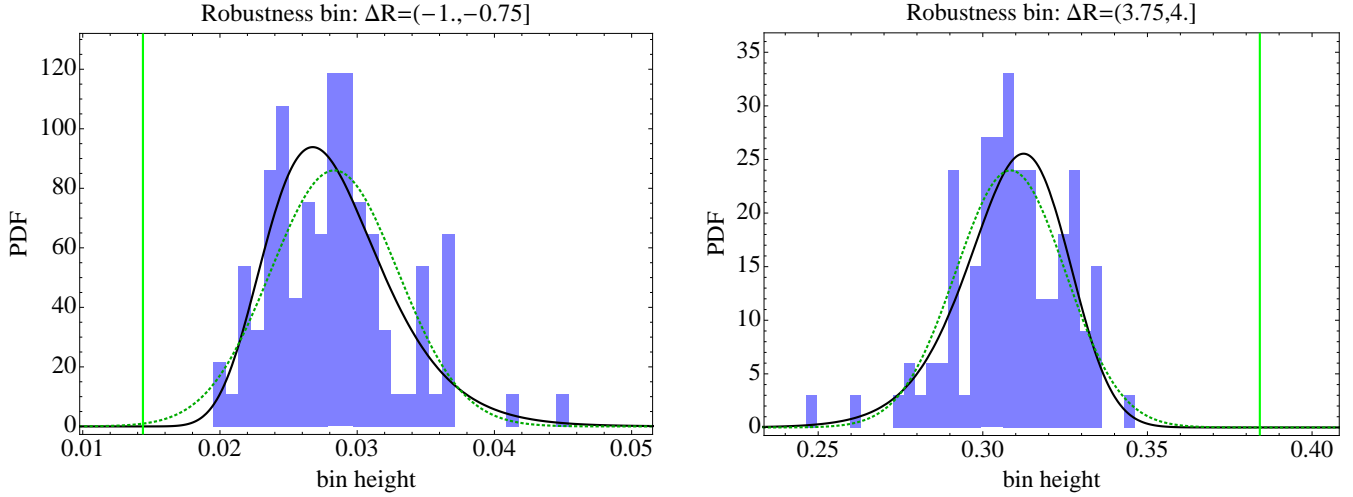


Figure 10. Same as Fig. 5 for the dataset \mathcal{D}_{U+} . The bin height corresponding to \mathcal{D}_{U+} is shown as a green vertical line, and corresponds to the green curve in Fig. 9. These two robustness bins were chosen for this plot as they quite strongly show that \mathcal{D}_{U+} is systematics driven. More precisely, the \mathcal{D}_{U+} datum relative to the bin $(3.75, 4]$ lies at $5.4\text{-}\sigma$ confidence levels. See Section 4.2 for more details.

to a dataset for which one indeed expects *a priori* a significant amount of contamination due to systematics. Luckily one such sample is readily available. The Union2.1 catalogue was in fact constructed by enforcing group quality criteria to their full supernova set of 753 elements, which resulted in the removal of 173 SNIa. The criteria were (Suzuki et al. 2012):

- (i) that the CMB-centric redshift is greater than 0.015;
- (ii) that there is at least one point between -15 and 6 restframe days from B-band maximum light;
- (iii) that there are at least five valid data points;
- (iv) that the entire 68% confidence interval for the SALT2 parameter x_1 lies between -5 and $+5$;
- (v) data from at least 2 bands with rest-frame central wavelength coverage between 2900 \AA and 7000 \AA ;
- (vi) at least one band redder than rest-frame U-band.

Now, these 173 SNIa are precisely ones for which systematics could be a dominant factor. However, for 38 of these the lightcurve fitter algorithm did not converge, so we do not have a measurement of their distance moduli. We thus analyzed the Union2.1 catalogue augmented with 135 supernovae that did not pass their quality cuts. We show these excluded supernovae in Fig. 8. We will refer to this dataset of 715 SNe as \mathcal{D}_{U+} .

As before, we have normalized both \mathcal{D}_{U+} and relative mocks to $\bar{\chi}^2 = 1$. The dataset \mathcal{D}_{U+} has indeed a very high $\bar{\chi}^2 = 1.72$ which, in order to go to unity, needs a quite large added error of $\sigma_{\text{int}}^{\text{extra}} = 0.070$ magnitudes. We show the results in Fig. 9, which has been obtained using the Pearson distribution (for both left and right panels) as explained in Section 4.1.2. As compared to the analysis of \mathcal{D}_{EdS} of Fig. 4, we have used a finer binning in the robustness. Now indeed the signal is in the body of the iR-PDF and not in the tail. The reason for this different behavior is that

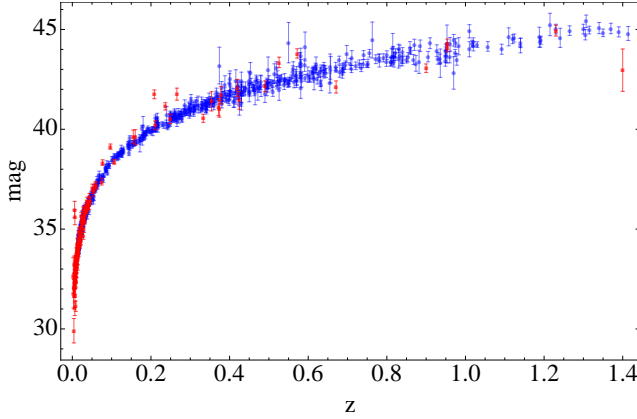


Figure 8. Plotted is the distance modulus of the SNe that passed the quality cuts (blue) and made it into the final Union 2.1 catalogue, and the distance modulus of the SNe that did not (red). See Section 4.2 for more details.

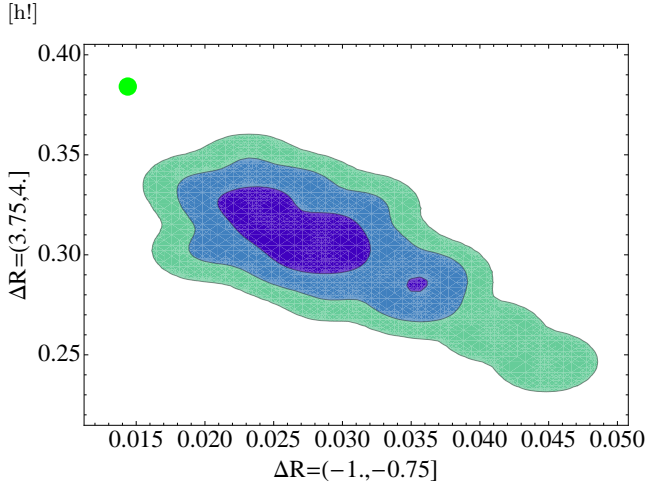


Figure 11. Same as Fig. 6 for the two robustness bins of Fig. 10. The bin height corresponding to \mathcal{D}_{U+} is shown as a green disk. See Section 4.2 for more details.

generally, by decreasing the value of $\bar{\chi}^2$, one makes the iR-PDF more peaked and with a shorter low-robustness tail. Therefore, in order to put the large $\bar{\chi}^2$ of \mathcal{D}_{U+} to unity, the latter catalogue has been “over normalized”, probably because the high value of $\bar{\chi}^2 = 1.72$ was due to just a bunch of very biased supernovae. From the results of Fig. 9 we can claim a detection at more than 3σ of the catalogue as being systematics-driven, which is a completely independent check that the SNe that did not pass the quality cuts were indeed dominated by systematic effects.

We show in Fig. 10 the distributions of the bin heights for two robustness bins that have a strong exclusion signal. We have plotted both the fitted Pearson distribution used in Fig. 9 and the fitted gaussian distribution for comparison. The \mathcal{D}_{U+} datum relative to the bin $(3.75, 4]$ lies at 5.4σ confidence levels. By estimating the uncertainty on the exclusion signal as explained at the end of Section 4.1.2, we find that the signal is $> 3.8\sigma$ at 95% confidence level.

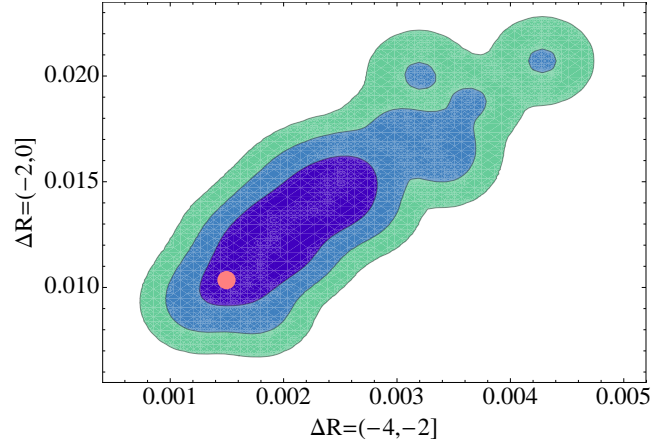


Figure 14. Same as Fig. 6 for the two robustness bins of Fig. 13. The bin height corresponding to \mathcal{D}_U is shown as a pink disk. See Section 4.3 for more details.

Finally, in Fig. 11 we show the contour plot of the correlated binned distribution of bin heights for the two robustness bins of Fig. 10. As before, we show this figure to illustrate the correlation between bins with strong signal, but we do not use it to assess the statistical properties of \mathcal{D}_{U+} as we only have a limited sample of mock catalogues.

4.3 Union2.1 dataset

Now that we have tested the sensitivity of the internal robustness method, we will show the results for the actual Union2.1 catalogue, to which we will refer as \mathcal{D}_U . Fig. 12 shows that we did not find any sign of systematic effects in the Union2.1 compilation. As Union2.1 is constructed from a collection of different instruments, it is a valid concern whether systematics are properly accounted for. For instance, individual estimations for the Malmquist bias in each of the supernova sub-samples were not made (Kowalski et al. 2008) and in general all systematics were treated by adding nuisance parameters (Suzuki et al. 2012). Moreover, their data in the compact form here used, which provides directly the distance moduli, assumes a particular cosmological model (the SALT2 parameters α and β are fixed in the best fits values given by such model) and is thus not technically independent data, as instead we implicitly assumed here. Our results are nevertheless clear, and serves as a cross-check on this compilation. This is one of the main results of this work.

As in the previous Sections, we show in Fig. 13 the distributions of the bin heights for two robustness bins that have the strongest signal. Again, we have plotted both the fitted Pearson distribution used in Fig. 12 and the fitted gaussian distribution for comparison. Note that, similarly to Fig. 4, in the left panel of Fig. 12 the gaussian distribution has been used. The latter is indeed a good template PDF for the robustness bins in the body with values $0 < R < 6$. In Fig. 14 we show the contour plot of the correlated binned distribution of bin heights for the latter two robustness bins. As before, we show this figure to illustrate the correlation between bins with strong signal.

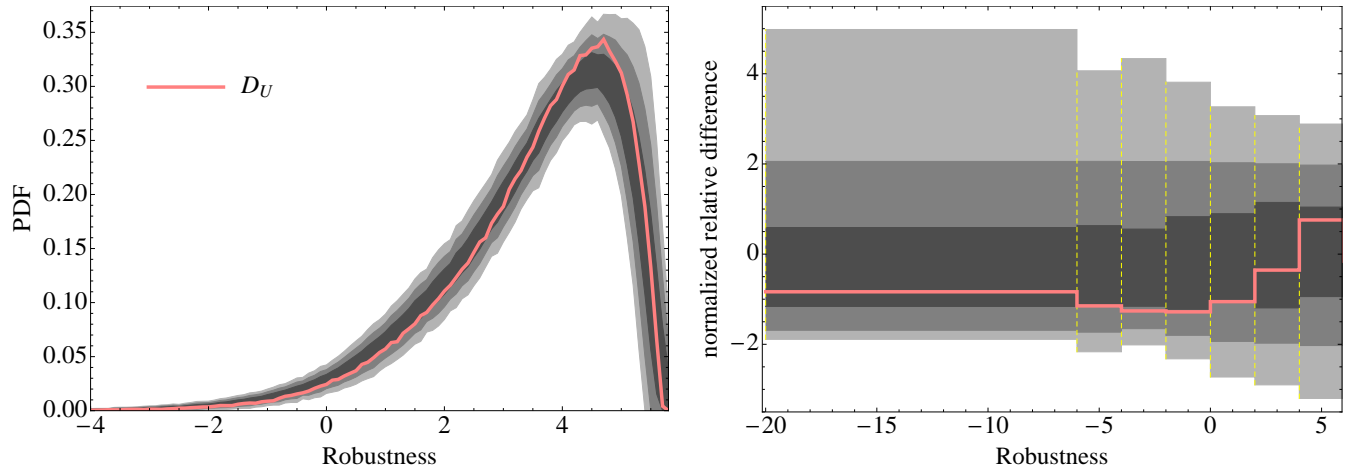


Figure 12. Same as Fig. 4 for the dataset \mathcal{D}_U (pink curve). These plots show that we did not find any sign of systematic effects in the Union 2.1 catalogue. See Section 4.3 for more details.

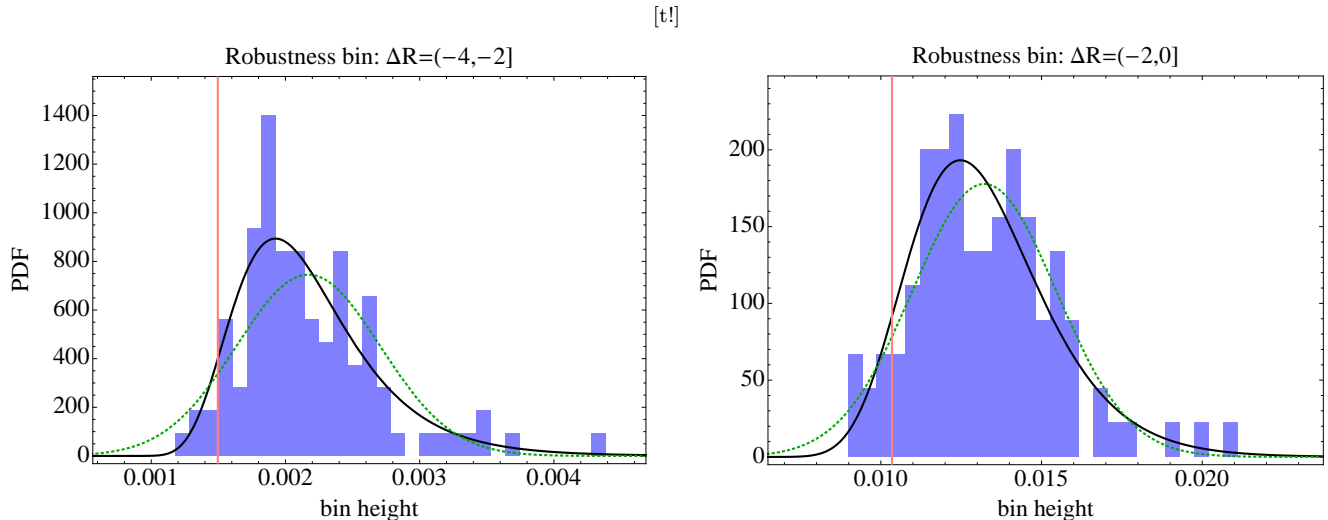


Figure 13. Same as Fig. 5 for the dataset \mathcal{D}_U . The bin height corresponding to \mathcal{D}_U is shown as a pink vertical line, and corresponds to the pink curve shown on the right panel of Fig. 12. These two robustness bins were chosen for this plot as they have the strongest (even though still weak) signal. See Section 4.3 for more details.

5 CONCLUSIONS

In this paper we proposed a new Bayesian statistical method, dubbed Internal Robustness, to detect the presence of systematics with an automated procedure. While a clear physical understanding of all effects contributing to any cosmological observation is our ultimate goal, we are still far from that level and must thus resort to statistical inference to guide us. Once identified, systematic-contaminated data can be further analyzed and eventually corrected (or at least excluded). Fig. 3 nicely summarizes the ultimate goal of internal robustness, that is, to go from the original set in green to the “decontaminated” set in blue. The contours do not look significantly different (i.e. same precision), but their position has substantially moved of $\sim 3\sigma$ (i.e. much better accuracy).

In order to test this method we applied it to three supernova catalogues, all based on the Union2.1 dataset: the

artificial \mathcal{D}_{EdS} (with 100 mock supernovae drawn from the “wrong” EdS model); the dataset \mathcal{D}_{U+} which includes supernovae that were previously excluded (because they were suspected of being dominated by systematics); and the “normal” catalogue \mathcal{D}_U (the standard Union2.1). The latter, nevertheless, is constructed from an assortment of different instruments, both ground and space based, and it is not completely clear *a priori* whether it would exhibit signs of (leftover) systematic effects.

Our results clearly show no evidence for systematic contamination in the standard Union2.1 data. This is an important result in itself and it serves as a cross-check on this very heterogeneous SNe compilation. For the other two catalogues, the results are also telling. Using a Pearson template to fit the distribution of mock data, we find robustly that the \mathcal{D}_{EdS} and \mathcal{D}_{U+} catalogues are systematics-driven at over $3.3\text{-}\sigma$ and $3.8\text{-}\sigma$ confidence level, respectively.

In the present paper we have focused on assessing if

a given dataset is dominated by systematics or not. If a catalogue does not pass the internal robustness test, then the next step would be to find the subsets of data that are most probably contaminated. To accomplish the latter one needs an efficient algorithm to find partitions with values of internal robustness as low as possible. Once the contaminated data are found they could be used to help test some suggested hypothesis, such as the existence of two distinct supernova populations, the evolution of the supernova intrinsic luminosity with redshift and/or host metallicity *et cetera*. We will address this issue in forthcoming work.

Although we selected supernovae as our testbed, the Internal Robustness method could be applied to any data, especially if one has reasons to suspect that the data come from two or more distinct populations. The scope of application is analogous to the standard goodness-of-fit tests, which the proposed method generalizes, and we are curious to see what it will tell when applied to other observables.

ACKNOWLEDGMENTS

It is a pleasure to thank Juan Garcia-Bellido, Caroline Heneka, Natallia Karpenka, Richard Kessler, Bruno Lago, Michele Maltoni, Savvas Nesseris, Ribamar Reis, Ignacy Sawicki and Wessel Valkenburg for fruitful discussions. LA and VM acknowledge support from DFG through the TRR33 program “The Dark Universe”. MQ is grateful to Brazilian research agency CNPq for support and to ITP, Universität Heidelberg for hospitality during part of the development of this project.

References

- Abell P. A., et al., 2009
 Amendola L., Kainulainen K., Marra V., Quartin M., 2010, Phys.Rev.Lett., 105, 121302
 Amendola L., Tsujikawa S., 2010, Dark Energy: Theory and Observations
 Antoniou I., Perivolaropoulos L., 2010, JCAP, 1012, 012
 Astier P., et al., 2006, Astron. Astrophys., 447, 31
 Bassett B. A., Fantaye Y., Hlozek R., Kotze J., 2011, Int.J.Mod.Phys., D20, 2559
 Bernstein J., Kessler R., Kuhlmann S., Spinka H., 2009
 Blake C., Davis T., Poole G., Parkinson D., Brough S., et al., 2011, Mon.Not.Roy.Astron.Soc., 415, 2892
 Carretta E., Gratton R. G., Clementini G., Fusi Pecci F., 2000, Astrophys.J., 533, 215
 Colin J., Mohayaee R., Sarkar S., Shafieloo A., 2011, Mon.Not.Roy.Astron.Soc., 414, 264
 Conley A., Guy J., Sullivan M., Regnault N., Astier P., et al., 2011, Astrophys.J.Suppl., 192, 1
 Eisenstein D. J., et al., 2005, Astrophys. J., 633, 560
 Garcia-Bellido J., Haugboelle T., 2008, JCAP, 0804, 003
 Graham P. W., Harnik R., Rajendran S., 2010, Phys.Rev., D82, 063524
 Guy J., Astier P., Baumont S., Hardin D., Pain R., et al., 2007, Astron.Astrophys., 466, 11
 Guy J., Sullivan M., Conley A., Regnault N., Astier P., et al., 2010, Astron.Astrophys., 523, A7
 Hansen B. M., Brewer J., Fahlman G. G., Gibson B. K., Ibata R., et al., 2002, Astrophys.J., 574, L155
 Hicken M., Wood-Vasey W. M., Blondin S., Challis P., Jha S., et al., 2009, Astrophys.J., 700, 1097
 Howell D. A., 2011, Nature Commun., 2, 350
 Jackson J., 2012
 Jha S., Riess A. G., Kirshner R. P., 2007, Astrophys.J., 659, 122
 Jimenez R., Thejll P., Jorgensen U., MacDonald J., Pagel B., 1996, Mon.Not.Roy.Astron.Soc., 282, 926
 Kainulainen K., Marra V., 2009, Phys.Rev., D80, 123020
 Kainulainen K., Marra V., 2011a, Phys.Rev., D83, 023009
 Kainulainen K., Marra V., 2011b, Phys.Rev., D84, 063004
 Kim A., 2011
 Koivisto T. S., Mota D. F., Quartin M., Zlosnik T. G., 2011, Phys.Rev., D83, 023509
 Komatsu E., et al., 2011, Astrophys.J.Suppl., 192, 18
 Kowalski M., et al., 2008, Astrophys.J., 686, 749
 Lago B., Calvao M., Joras S., Reis R., Waga I., et al., 2011, Astronomy & Astrophysics, 541, A110
 Lampeitl H., Nichol R., Seo H., Giannantonio T., Shapiro C., et al., 2009, Mon.Not.Roy.Astron.Soc., 401, 2331
 Maltoni M., Schwetz T., 2003, Phys.Rev., D68, 033020
 Maltoni M., Schwetz T., Tortola M., Valle J., 2002, Nucl.Phys., B643, 321
 March M., Trotta R., Amendola L., Huterer D., 2011, Mon.Not.Roy.Astron.Soc., 415, 143
 March M., Trotta R., Berkes P., Starkman G., Vaudrevange P., 2011
 Marra V., Notari A., 2011, Class.Quant.Grav., 28, 164004
 Marriner J., et al., 2011, Astrophys.J., 740, 72
 Marshall P., Rajguru N., Slosar A., 2006, Phys.Rev., D73, 067302
 Pearson K., 1895, Royal Society of London Philosophical Transactions Series A, 186, 343
 Pearson K., 1916, Royal Society of London Philosophical Transactions Series A, 216, 429
 Perlmutter S., et al., 1999, Astrophys. J., 517, 565
 Riess A. G., et al., 1998, Astron. J., 116, 1009
 Suzuki N., Rubin D., Lidman C., Aldering G., Amanullah R., et al., 2012, Astrophys.J., 746, 85
 Trotta R., 2008, Contemp.Phys., 49, 71

APPENDIX A: TECHNICAL DETAILS

While scanning supernova subsets and building the robustness histogram, one has to carefully analyze small subsets. These small subsets produce indeed contours which are not only very broad but also have best-fit values very far from typical ones obtained with the full catalog. In the $\{\Omega_{m0}, \Omega_{\Lambda0}\}$ parameter space this entails some technical problems.

One issue has to do with “no Big-Bang” scenarios. For any positive value of Ω_{m0} there exists a positive value of $\Omega_{\Lambda0}^{\max}$ for which the Hubble function $H(z)$ goes to zero at a finite redshift. This $\Omega_{\Lambda0}^{\max}(\Omega_{m0})$ line is usually referred to as the no-Big-Bang line (or “loitering” line), values of $\Omega_{\Lambda0}$ above which are excluded. The same issue arises for any negative value of Ω_{m0} , although this is usually correctly perceived as an unimportant technicality as a negative Ω_{m0} is

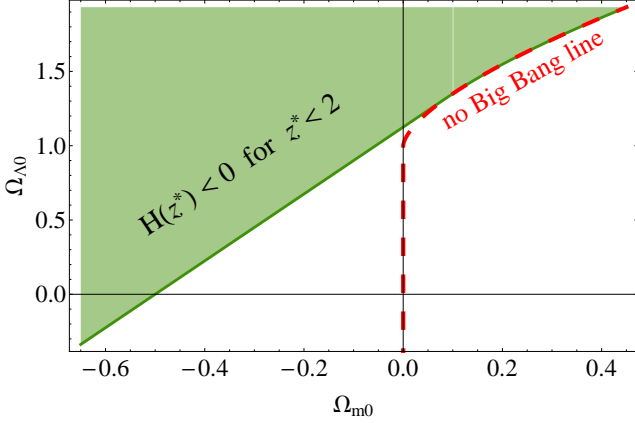


Figure A1. Shown is the excluded parameter-space region (green shaded area) for which the expansion rate is negative for $z < 2$. This ensures that the distance (proportional to $\int dz/H(z)$) to a source at redshift $z < 2$ is not singular. This is a relaxation of the usual no-big-bang region (left of the red dashed line). See Appendix A for more details.

physically excluded *a priori*. Here, on the other hand, allowing negative Ω_{m0} is reasonable as it will be a hint that systematics are involved (we may be misinterpreting a systematic parameter for Ω_{m0} – see Section 2.4). Likewise, a likelihood that embraces values of $\Omega_{\Lambda0} > \Omega_{\Lambda0}^{\max}$ may also be a hint of hidden systematics.

In order to allow as much freedom as possible to the likelihood contours, we adopted an “extended” no-Big-Bang line: we allow values of $\{\Omega_{m0}, \Omega_{\Lambda0}\}$ that do not exhibit a singularity in $H(z)$ for $z < 2$. This encompasses all supernovae measured so far and opens up a large region for which $\Omega_{m0} < 0$; see Fig. A1.

To find the line that delimits such a region one computes first the solutions $\Omega_{\Lambda0}^{\max}(z, \Omega_{m0})$ for which $H(z) = 0$. The minimum of $\Omega_{\Lambda0}^{\max}(z, \Omega_{m0})$ with respect to z gives the lower redshift for which $H(z) = 0$ for a given Ω_{m0} . The function we are looking for is then $\Omega_{\Lambda0}^{\max}(z^*(\Omega_{m0}), \Omega_{m0})$ where $z^*(\Omega_{m0})$ is either the redshift corresponding to the minimum $z_m(\Omega_{m0})$ or 2, whichever is lower. In other words, $z^* = \text{Min}(z_m, 2)$. Carrying out this calculation one gets

$$\Omega_{\Lambda0}^{\max}(\Omega_{m0}) = \begin{cases} \frac{9}{8}(1 + 2\Omega_{m0}), & \Omega_{m0} \leq 1/10; \\ \Omega_{\Lambda0}^{\text{noBB}}(\Omega_{m0}), & \Omega_{m0} \geq 1/10; \end{cases} \quad (\text{A1})$$

where $\Omega_{\Lambda0}^{\text{noBB}}$ is the traditional no Big Bang function:

$$\begin{aligned} \Omega_{\Lambda0}^{\text{noBB}}(x) = & \left[4x^4 + 4x^2(1+y) - 4x^{11/3}(1-x+y)^{1/3} \right. \\ & + x^{4/3}y(1-x+y)^{2/3} + 4x^{10/3}(1-x+y)^{2/3} \\ & - 4x^3(2+y) - x^{7/3}(2+y)(1-x+y)^{2/3} \\ & + x^{8/3}(1-x+y)^{1/3}(4+3y) \\ & \left. + \left(x^4(x^2 + 2(1+y) - 2x(2+y)) \right)^{1/3} \right] \\ & \times \left[x^{4/3}(1-x+y)^{1/3} \left(x^{4/3} + (x(1-x+y))^{2/3} \right. \right. \\ & \left. \left. + (x^2 + 2(1+y) - 2x(2+y))^{2/3} \right) \right]^{-1}, \end{aligned}$$

where in turn $x = \Omega_{m0}$ and $y \equiv \sqrt{1 - 2x}$.

This paper has been typeset from a T_EX/ L^AT_EX file prepared by the author.